Materials Research Express

PAPER

Ferromagnetic behavior of native point defects and vacancy-clusters in ZnO studied by first principle calculation

Cai-Qin Luo[1,2], **Si-Cong Zhu**[3], **Chi-Hang Lam**[4] and **Francis Chi-Chung Ling**[1]

[1] Department of Physics, The University of Hong Kong, Pokfulam Road, Hong Kong, People's Republic of China
[2] Henan Key Laboratory of Photovoltaic Materials, Henan University, Kaifeng, People's Republic of China
[3] College of Science and Key Laboratory for Ferrous Metallurgy and Resources Utilization of Ministry of Education, Wuhan University of Science and Technology, Wuhan, People's Republic of China
[4] Department of Applied Physics, Hong Kong Polytechnic University, Hung Hom, Hong Kong, People's Republic of China

E-mail: ccling@hku.hk

OPEN ACCESS

RECEIVED
7 April 2020

REVISED
27 June 2020

ACCEPTED FOR PUBLICATION
30 June 2020

PUBLISHED
8 July 2020

Keywords: ZnO, ferromagnetism, first principle calculation, native point defects, vacancy clusters

Abstract

The origin of room temperature ferromagnetism in undoped ZnO is still a question of debate. Experimental and theoretical findings are inconclusive as to the predominant contributor for the magnetic behavior of undoped ZnO. First principle calculation pseudopotential method was used to systematically determine the relaxed atomic geometry, the formation energies and the magnetic properties of the native point defects (vacancies, interstitials and antisites), and vacancy clusters ($V_{Zn}V_O$, $V_{Zn} - 2V_O$ and $2V_{Zn} - V_O$) in ZnO. The results show that ZnO cells consisting of the V_{Zn} and the O_i have non-zero magnetic moments, energetically favoring ferromagnetic states and close-to-room-temperature Curie temperatures (294 K). V_{Zn} and O_i are also characterized by their low formation energies, in particular in the case of n-type (i.e. Fermi level close to the conduction band minimum) and O-rich conditions. The energy differences between the ferromagnetic state and anti-ferromagnetic state for V_{Zn} and O_i are larger than kT at room temperature but still relatively small (~34 meV). Although V_{Zn} and O_i would contribute for the room temperature ferromagnetism, the ferromagnetism states would not be robustly stable for thermal excitation to the anti-ferromagnetic states.

Introduction

Diluted magnetic semiconductor (DMS) has been receiving extensive attention since Munekata *et al*'s first fabrication of (In, Mn)As DMS [1]. These fundamental studies of DMS have been of interest for the development of spintronic devices [2]. The electron spins in spintronic devices are exploited as a further degree of freedom, increasing the efficiency of the device of information storage. A commonly used technique to obtain DMS was to dope magnetic elements into a semiconductor material, such as TiO_2 [3], GaN [4] and ZnO [5]. Other than being the DMS, ZnO is also a multi-functional material suitable for a variety of applications like ultra-violet optoelectronic, transparent electrode, sensors, and photocatalysis [6], which thus attracts extensive focus of research activities. In recent years, Dietl *et al* [7] studied the Curie temperature T_C for different p-type semiconductors, found that room-temperature ferromagnetism (RTFM) can be realized in p-type ZnO doped by Mn. Despite numerous experimental observations of RTFM in transition metal (TM) doped ZnO, it is still uncertain as to what are the relevant origins of the RTFM in doped ZnO, which may be originated from the introduced dopant, the interaction between dopant and intrinsic defect, or second phase, etc. Most of the published work, based on theoretical calculation and experimental verification concluded that intrinsic defects play a crucial role in the magnetic behavior of doped ZnO. For example, Yi *et al* [8] proposed that RTFM observed in Li-doped ZnO may be associated with the V_{Zn} vacancy based on the results of positron annihilation spectroscopy (PAS) study. They also found that doping with appropriate dopants can lower the formation energy of V_{Zn}. Besides, V_O is also critical in one way or another on magnetic property. Hsu *et al* [9] found a

correlation between the enhancement of ferromagnetism and the increase of oxygen vacancies in Co-doped ZnO. By using soft x-ray absorption, x-ray magnetic circular dichroism and first-principle calculations, Herng *et al* [10] found both Cu impurities and V_O were essential to the observed RTFM in Cu doped ZnO and proposed an indirect exchange model as the cause.

RTFM has also been reported in undoped ZnO material with different structures [11–13]. Despite of many efforts devoted [14–18], the origin of the observed RTFM in undoped ZnO is still inconclusive. With the comprehensive study based on first-principle calculation and photoluminescence, the observed RTFM in ZnO nano-particles grown by a solution method was attributed to singly ionized oxygen vacancies [19]. Xing *et al* [19] reported RTFM in ZnO nanowires obtained by using a vapor transport method, and the magnetic property was tunable by adjusting the oxygen deficiency during growth. Using density functional theoretical (DFT) study, Wang *et al* [20] found that the FM in undoped ZnO could be attributed to V_{Zn} instead of V_O, also indicated V_{Zn} prefer to form clusters. Similarly, Chakrabarty and Patterson [21] carried out a DFT study and suggested that the RTFM in undoped ZnO could originate from the isolated V_{Zn}^{-} and ($V_{Zn}V_O$)-divacancy. With molecular dynamics and DFT studies, Tietze *et al* [22] showed the presence of unpaired electrons at the grain boundary and these unpaired electrons were ferromagnetically coupled. Most of the RTFM theoretical studies of native defects in undoped ZnO focused on V_{Zn}, V_O, and $V_{Zn}V_O$ divacancy. It is no doubt that, under equilibrium condition, V_{Zn} and V_O are the predominant defects due to their relatively low formation energies [23]. However, for ZnO samples undergone non-equilibrium process, e.g. electron irradiation [24, 25] and ion implantation [26, 27], other kinds of intrinsic defects and vacancy clusters having higher formation energies would exist. It is thus also important to understand the magnetic properties of these defects to grip a more comprehensive view for interpreting the experimental data.

Using the density functional theory (DFT) method, we studied the relaxed atomic geometry, the formation energy and magnetic properties for all the native point defects (vacancies, interstitials and antisites) and vacancy clusters ($V_{Zn}V_O$, $2V_{Zn} - V_O$ and $2V_O - V_{Zn}$) in ZnO so as to gain the knowledge of their roles in ZnO materials exhibiting RTFM.

Method

All calculations in the present study were performed based on DFT, using the projector augmented wave method (PAW) as implemented in the Vienna *ab initio* Simulation Package. The exchange-correlation potential was represented by the spin-polarized generalized gradient approximation (SGGA). The plane wave cut-off energy was taken as 400 eV throughout the calculation. All the atoms in the supercell were fully relaxed until the Hellmann-Feynman force converged to less than 0.01 eV A^{-1}. For the k-space integration, a $3 \times 3 \times 3$ k-points grid was used for sampling the irreducible wedge of the Brillouin zone. Test calculation for the selection of cut-off energy and k-points were performed, finding that the results remained unchanged with higher cutoff energy and denser k-points. A homogeneous background-charge was added or removed from the supercell to obtain the different charge states of the defects.

The present study covered all the relevant charge states of V_O, V_{Zn}, Zn_O, O_{Zn}, Zn_i, O_i, $V_{Zn}V_O$, $V_{Zn} - 2V_O$ and $2V_{Zn} - V_O$. The total energies for the different defect configurations were calculated to yield the formation energies. The equilibrium defect concentration c depends on the formation energy and is given by: $c = N_{sites} \exp\left(-\frac{E^f}{k_B T}\right)$, where N_{sites} is the number of the possible defect sites in the supercell, E^f is the formation energy, and k_B is Boltzmann constant. The formation energy can be found by calculating the total energy of the supercell, as given by [28]:

$$E^f(X^q) = E_{tot}(X^q) - E_{tot}(ZnO, perfect) - \sum_i n_i \mu_i + q(E_V + E_F). \quad (1)$$

q is the charge state of the defects and $E^f(X^q)$ is the formation energy of the defect X in the supercell. $E_{tot}(X^q)$ is the total energy obtained from the DFT calculation for defect X with the charge state of q, $E_{tot}(ZnO, perfect)$ is the total energy of the defect-free ZnO supercell, n_i is the number of atoms (type i) that have been added ($n_i < 0$) or removed ($n_i > 0$) from the supercell. μ_i is the chemical potential of the element i, E_F is the Fermi-level. E_v is the valance band maximum of ZnO, which is given as: $E_v = E_{tot}^{q=0}(\mathrm{ZnO},\ defect\ free) - E_{tot}^{q=1}(\mathrm{ZnO},\ defect\ free)$. The chemical potential μ_i depends on the Zn and O stoichiometries and bounds for the chemical potentials were set for the conditions of Zn-rich and O-rich. As the chemical potential for Zn (μ_{Zn}) cannot be larger than that of Zn bulk, the maximum bound for the chemical potential of Zn ($\mu_{Zn}^{\max}$) was taken as the Zn bulk value for the Zn-rich condition. Similarly, under the O-rich condition, the upper limit of the chemical potential of O ($\mu_{\mathrm{Zn}}^{\min}$) is bounded by half of the total energy of the O_2 molecule. The entropy of formation is given by $\Delta H_f(\mathrm{ZnO}) = \mu_{Zn} + \mu_O$ and was found to be −3.5 eV in the present study. Therefore, the lower limit on μ_{Zn} and μ_O can be

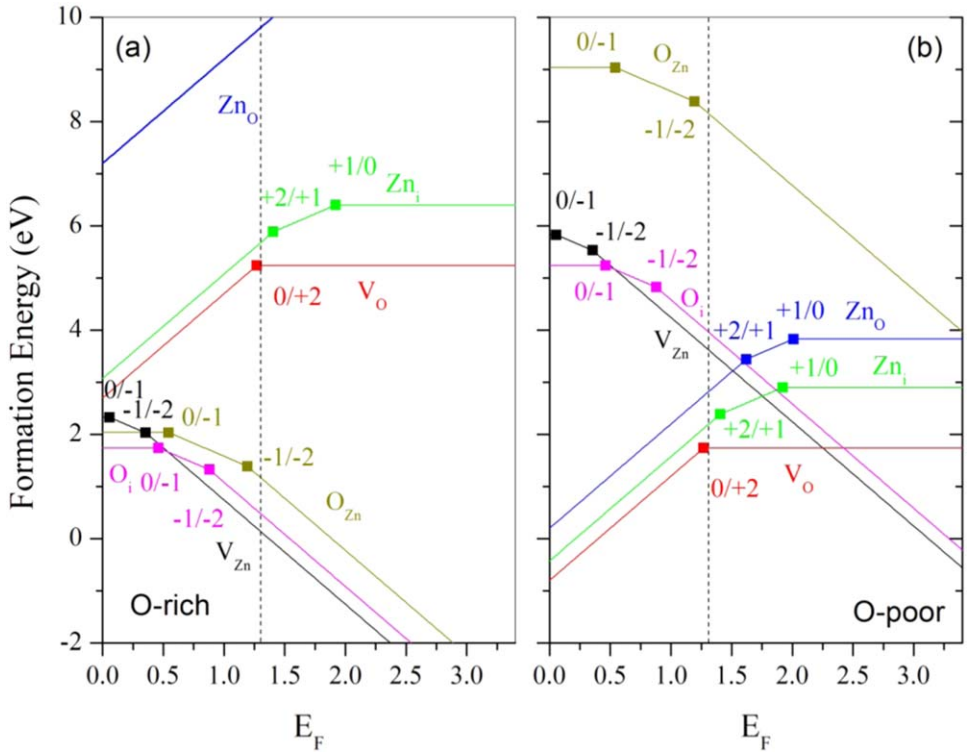

Figure 1. Formation energies of native point defects in their relevant charge states in ZnO as a function of the Fermi-level in (a) O-rich condition and (b) O-poor condition. $E_F = 0$ refers to the valence-band maximum. Only the lowest formation energies of defects in different charge states are shown. The point at the line indicates the transition level of the defect.

described as $\mu_{Zn}^{min} = \Delta H_f\,(ZnO) - \mu_O^{max}$ and $\mu_O^{min} = \Delta H_f\,(ZnO) - \mu_{Zn}^{max}$ respectively for the O-rich and Zn-rich conditions respectively.

Results

Structural relaxation

All atoms in the supercell are fully relaxed during the optimized procedure. It is worthy to discuss the relaxation of the vacancies. For the neutral and +1 states of V_O, the nearest Zn atoms respectively displaced inward by 12.3% and 0.3% as compared with the equilibrium Zn-O bond length. For the +2 charge states of V_O, the neighboring Zn atoms displaced outward by 24%. For V_{Zn} with neutral, −1 and −2 charge states, the relaxations were similar, i.e. 10.6% outward as compared to the equilibrium Zn–O bond length. Vacancy clusters are formed through removing the nearest neighboring atoms in the perfect supercell with the equilibrium Zn–O bond length of 1.98 Å respectively on the a-b basal plane and along the *c*-axis. For $V_O - V_{Zn}$, both O atoms and Zn atoms neighboring the defect exhibited outward displacement. The most significant outward displacement occurred on the charge state of $(V_{Zn} - V_O)^{+1}$. The nearest O atoms displaced outward by 6.2% at the basal plane and 16% along the *c*-axis, while the surrounding Zn atoms displaced outward by 4% along the *c*-axis and no obvious displacement at the a-b basal plane. For the $2V_O - V_{Zn}$ and $2V_{Zn} - V_O$ clusters, three nearest atoms were removed in a perfect supercell. The outward displacements for O and Zn atoms around the vacancy clusters are basically similar to that for $V_O - V_{Zn}$, whereas the nearest O atoms along the c-axis had the most significant outward displacement.

Formation energies

The formation energies of the different intrinsic point defects (namely V_{Zn}, V_O, Z_{ni}, O_i, Zn_O , and O_{Zn}) against the Fermi level positive (measured from the valance band minimum) obtained from the DFT calculation are shown in figure 1. The interstitial defects have two configurations in the wurtzite structure, namely the octahedral coordinated (oct) site and the tetrahedral coordinated (tet) site [23]. The oct-site usually has lower formation energy than that for the tet-site. Therefore, only the low-formation-energy oct-site was studied in the present study. The valence band maximum (VBM) is set to be at 0 eV, whereas the theoretical conduction band minimum (CBM) is indicated by the black dotted line in figure 1. The Fermi-level E_F varies from the valence band edge to the experimental conduction band edge, for which the experimental band gap was obtained by

Table 1. Shows the formation energies of native point defects with the relevant charge states in ZnO. These values are given for the O-rich and O-poor conditions, and Fermi-levels at the top of the valence band ($E_F = 0$ eV) and at the bottom of the conduction band ($E_F = 3.4$ eV).

		O-rich condition		Zn-rich condition	
Defect	Charge state	VBM	CBM	VBM	CBM
V_{Zn}	0	2.33	2.33	5.83	5.83
	1−	2.39	−1.01	5.89	2.49
	2−	2.74	−4.06	6.24	−0.56
V_O	0	5.24	5.24	1.74	1.74
	1+	4.13	7.53	0.63	4.03
	2+	2.70	9.50	−0.80	6.00
O_{Zn}	0	2.04	2.04	9.04	9.04
	1−	2.58	−0.82	9.58	6.18
	2−	3.78	−3.02	10.78	3.98
Zn_O	0	10.83	10.83	3.83	3.83
	1+	8.82	12.22	1.82	5.22
	2+	7.20	14.00	0.20	7.00
Zn_i (oct)	0	6.40	6.40	2.90	2.90
	1+	4.48	7.88	0.98	4.38
	2+	3.07	9.87	−0.43	6.37
O_i (oct)	0	1.74	1.74	5.24	5.24
	1−	2.20	−1.20	5.70	2.30
	2−	3.08	−3.72	6.58	−0.22

optical transmittance measurement. The charge state transition levels of the defects are indicated by the square points in figure 1. Table 1 tabulates the formation energies for the different native point defects in the different relevant charge states as the E_F is at the VBM and CBM. Under the O-rich condition, the V_{Zn}, O_i and O_{Zn} acceptors have low formation energies for n-type ZnO materials with E_F in the upper-half mid-gap close to the conduction band (as shown in figure 1(a)). Under the O-poor condition (as shown in figure 1(b)), V_{Zn} and O_i have lower formation energies than the other defects as E_F is close to the CBM (i.e. n-type material); while V_O, Zn_i and Zn_O have lower formation energies with E_F laying close to the VBM (i.e. p-type material). The results found in the present calculation are in agreement with the findings in the most studies reported in the literature [23, 29, 30].

The formation energies for the vacancy cluster, namely $V_{Zn}V_O$, $2V_{Zn} - V_O$ and $2V_O - V_{Zn}$, with the different charge states were calculated, and their formation energies against the E_F position in the O-rich and O-poor conditions are shown in figures 2(a) and (b) respectively. Table 2 tabulates the formation energies of vacancy cluster defects in the O-rich and O-poor conditions while the E_F is at the VBM and CBM. The tri-vacancy clusters $2V_O - V_{Zn}$ and $2V_{Zn} - V_O$ have two different configurations, namely laying on the a-b plane and along the *c*-axis, for which their formation energies are shown in figure 2 by the solid line and dashed line respectively. It is noticed that $2V_O - V_{Zn}$ and $2V_{Zn} - V_O$ staying at the a-b plane has lower formation energies as compared to those along the *c* axis. For n-type environment with E_F close to the CBM, the formation energies descend from $2V_O - V_{Zn}$, $V_{Zn}V_O$, to $2V_{Zn} - V_O$ for both the O-rich and O-poor conditions. Among the vacancy clusters, $2V_{Zn} - V_O$ in both the configurations of a-b plane and *c*-axis have the lowest formation energy, but are still significant higher than those of the intrinsic point defects having low formation energies like V_{Zn}, O_{Zn} and O_i(oct).

Magnetic properties

The total magnetic moments M_{total} of the unit cells containing the corresponding defects in the different charge states were calculated. All the Zn and O atom sites in the supercell were included to calculate for the total magnetic moments. The resultant total magnetic moments, as well as the corresponding contributions from Zn and O atoms, of the unit cell containing the defects having non-zero total magnetic moments are tabulated in table 3. The unit cells containing V_{Zn}, O_{Zn}, O_i (oct), $V_{Zn}V_O$, $2V_{Zn} - V_O$ (a-b plane) and $2V_{Zn} - V_O$ (c-axis) have non-zero magnetic moments for some of their charge states, while the unit cells containing V_O, Zn_O, Zn_i and $V_{Zn} - 2V_O$ do not have net total magnetic moment.

The energy difference between the spin-polarized state and non-polarized state was compared in the ZnO supercell (72 atoms) containing one defect. The spins on the Zn and O atoms neighboring the defect (parallel direction for ferromagnetic (FM) state and antiparallel arrangement for antiferromagnetic (AFM) state) were manually set. For the systems energetically favoring spin-polarized states, the total energy calculations of their

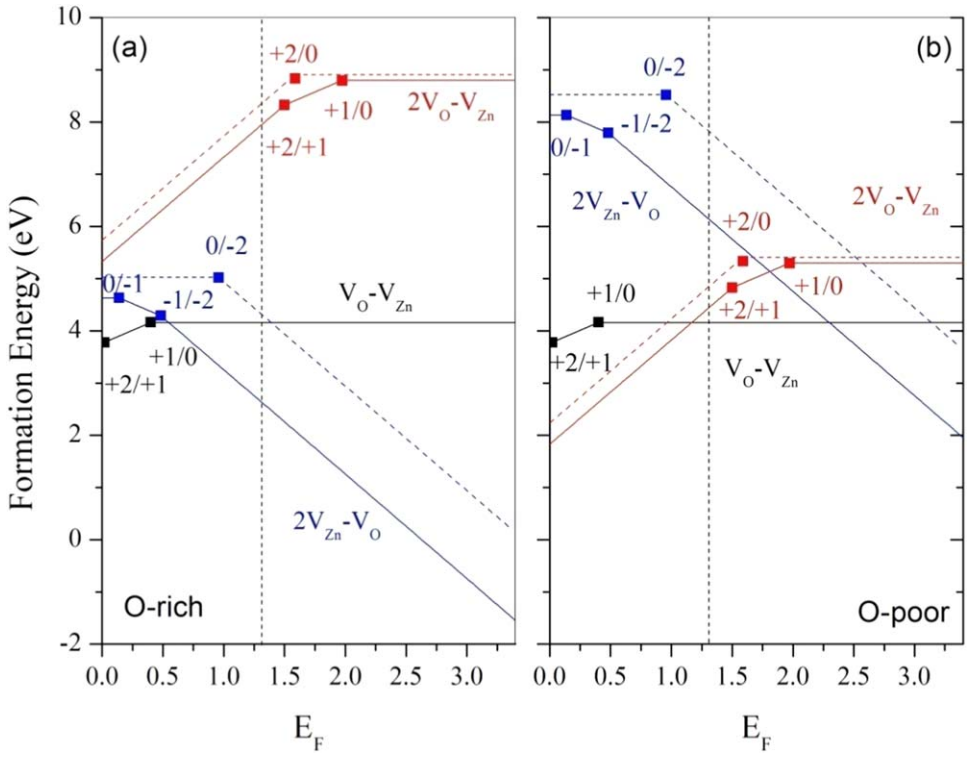

Figure 2. Formation energies of different vacancy clusters with their relevant charge states in ZnO as a function of the Fermi-level position under (a) O-rich condition; and (b) O-poor condition. The zero-point of the Fermi-level corresponds to the top of the valence-band. Only the lowest-energy states are shown. The square points indicate the transition levels in the band gap. For the $2V_{Zn} - V_O$ and $2V_O - V_{Zn}$ defects, the solid line indicates the defect staying at the a-b plane while the dashed line represents the defect along the *c* axis.

Table 2. Formation energies of vacancy clusters in ZnO supercell with the relevant charge states in ZnO. These values are given for the O-rich and O-poor conditions, and Fermi-level at the top of the valence band ($E_F = 0$ eV) and bottom of the conduction band ($E_F = 3.4$ eV).

			O-rich condition		Zn-rich condition	
Defect	orientation	Charge state	VBM	CBM	VBM	CBM
$V_O - V_{Zn}$	/	0	4.16	4.16	4.16	4.16
		1+	3.76	7.16	3.76	7.16
		2+	3.74	10.54	3.74	10.54
$2V_{Zn} - V_O$	*c* axis	0	5.03	5.03	8.53	8.53
		1−	6.40	3.00	9.9	6.50
		2−	6.94	0.14	10.44	3.64
$2V_{Zn} - V_O$	a-b plane	0	4.64	4.64	8.14	8.14
		1−	4.78	1.38	8.28	4.88
		2−	5.26	−1.74	8.76	1.76
$2V_O - V_{Zn}$	*c* axis	0	8.91	8.91	5.41	5.41
		1+	8.26	11.66	4.76	8.16
		2+	5.73	12.53	2.23	9.03
$2V_O - V_{Zn}$	a-b plane	0	8.80	8.80	5.30	5.30
		1+	6.83	10.23	3.33	6.73
		2+	5.33	12.13	1.83	8.63

FM and AFM states were extended to a larger unit cell with 144 atoms (i.e. having the size of the two original unit cells) with the separation between the defects being around 9.79 Å. The energy difference between the FM state and AFM state of the defects ($\Delta E = E_{AFM} - E_{FM}$) are tabulated in table 3. The energy differences E_{AFM}-E_{FM} are positive for V_{Zn}, O_i(oct), $2V_{Zn} - V_O$ (c-axis) and $2V_{Zn} - V_O$ (a-b plane), indicating that the FM ordering is energetically more stable than the AFM ordering for these defects. The $O_{Zn}{}^0$ and V_{Zn}-V_O^{2+} states have negative

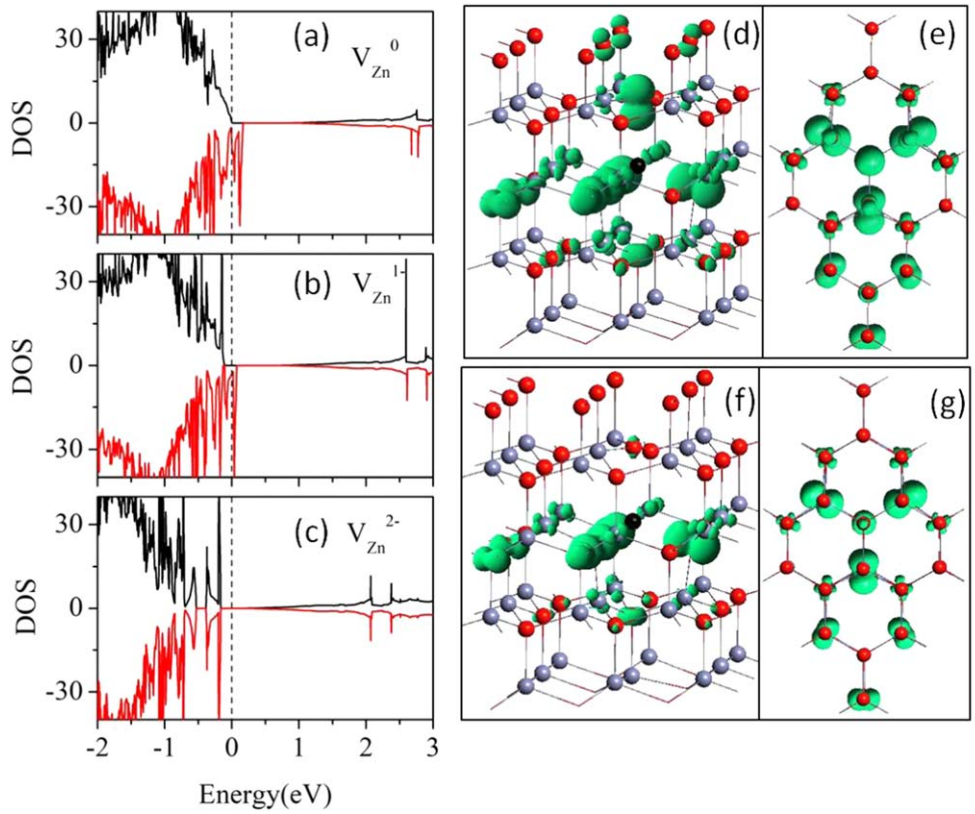

Figure 3. The DOS' of ZnO with the (a) V_{Zn}^{0}, (b) V_{Zn}^{1-} and (c) V_{Zn}^{2-}. The spin up (black line) and spin down (red line) DOS' is set above and below the abscissa axis. The Fermi-level is indicated by the black dash line at 0 eV. (d) The side view and (e) the top view of the effective spin density distribution for V_{Zn}^{0}. (f) The side view and (g) the top view of the effective spin density distribution for V_{Zn}^{1-}. The iso-surface value is 0.02 e A^{-3}. The black, red and black balls represent Zn, O and vacancy atoms in supercell respectively.

Table 3. The calculated magnetic moments (in μB) per unit cell (72 atoms) containing the corresponding defect. M_{total} is the total magnetic moment of the supercell. M_{Zn} and M_O are the contributions from the Zn site and O site. $\Delta E$is the energy difference between the AFM and FM ordering (E_{AFM}-E_{FM}), for which positive value indicates FM ordering is more stable while negative value indicates the defect prefer AFM ordering. Curie temperatures (T_C) calculated based on mean-field approximation were also included.

		Moment (μB)/Per Unit Cell				
	Charge	M_{total}	M_{Zn}	M_O	ΔE (meV)	T_C (K)
V_{Zn}	0	1.820	0.010	1.810	38	294
	1−	0.990	0.004	0.986	31	239
O_{Zn}	0	2.0	−0.01	2.01	−4	/
O_i(oct)	0	2.0	0.013	1.987	20	155
	1−	1.012	0.002	1.01	38	294
$V_{Zn} - V_O$	2+	1.384	0.034	1.350	−3	/
$2V_{Zn} - V_O$(c axis)	0	1.997	0.018	1.979	22	170
	1−	0.948	0.039	0.909	29	224
$2V_{Zn} - V_O$(a-b plane)	0	1.774	0.018	1.756	20	155
	1−	0.999	0.005	0.994	7	54

E_{AFM}-E_{FM} of −4 meV and −3 meV respectively, implying that their AFM states are relatively stable than the FM states.

It would be worthy to discuss the results of the defects carrying non-zero magnetic moment and energetically favoring FM state. The supercell containing the V_{Zn} and O_i (oct) acceptors have respectively the total moment of 1.82 μB and 2.0 μB for the neutral state, while they decrease to 0.99 μB and 1.012 μB if the charge state is −1. It is noticed that adding a hole to the neutral V_{Zn} and O_i acceptors leads to the increase of their magnetic moments. The magnetic moments contributed from the Zn-site and O-site (M_{Zn} and M_O respectively) as tabulated in table 1 show that the oxygen atoms give the major contribution for the total moments in the

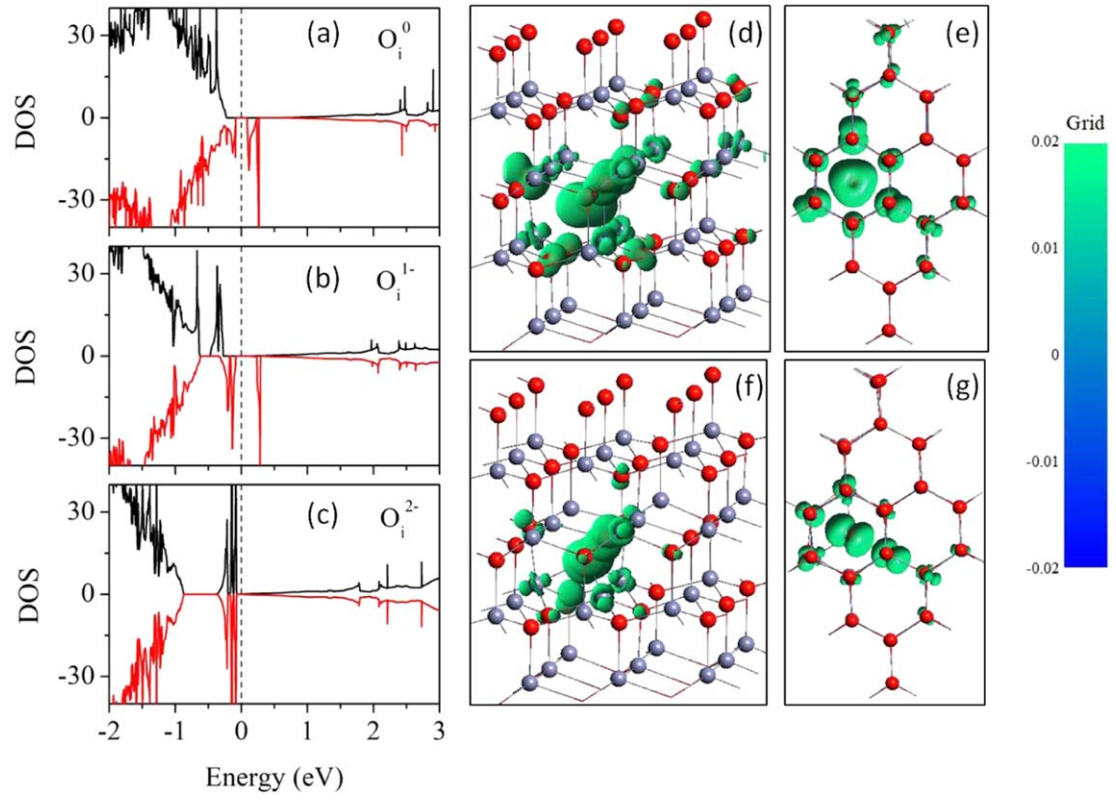

Figure 4. The DOS' of ZnO with the (a) O_i^0, (b) O_i^{1-} and (c) O_i^{2-}. The spin up (black line) and spin down (red line) DOS' is set above and below the abscissa axis. The Fermi-level is indicated by the black dash line at 0 eV. (d) The side view and (e) the top view of the effective spin density distribution for O_i^0. (f) The side view and (g) the top view of the effective spin density distribution for O_i^{1-}. The iso-surface value is 0.02 e A^{-3}. The black, red and black balls represent Zn, O and vacancy atoms in supercell respectively.

supercell. For the $2V_{Zn} - V_O$ cluster having the neutral charge, the defect staying along the *c* axis has a slightly larger magnetic moment than that at the a-b plane (namely 1.997 μB and 1.774 μB). For the $2V_{Zn} - V_O$ cluster having the 1− charge, the defect staying along the *c* axis has a negligibly smaller magnetic moment while compared to that at the a-b plane (namely 0.948 μB and 0.999 μB). It is also noticed that the $2V_{Zn} - V_O$ clusters in neutral charge have the smaller magnetic moment as compared to that in the 1− charge.

The Curie temperatures (T_C) were estimated by the mean-field approximation, which was given by: $T_C = \frac{2\Delta E}{3k_B}$ [31, 32]. The resultant Curie temperatures are tabulated in table 3. The ZnO supercells with the $V_{Zn}{}^0$ and the O_i^- (oct) have T_C's close to the room temperature which were 294 K. The Curie temperatures for $2V_{Zn} - V_O$'s with the different charge states and configurations were all below the room temperature.

The calculated total density of states (DOS) for the ZnO supercell (72 atoms) with a $V_{Zn}{}^0$, $V_{Zn}{}^-$ and $V_{Zn}{}^{2-}$ are shown in figures 3(a)–(c) respectively. The asymmetric spin-up and spin-down densities of $V_{Zn}{}^0$ and $V_{Zn}{}^{1-}$ in figures 3(a) and (b) show that the spin-up states are fully occupied but the spin-down states are partially filled. The $V_{Zn}{}^{2-}$ has symmetric spin up and down densities and thus its magnetic moment is zero. The side views and top views of the corresponding spin-density distributions for $V_{Zn}{}^0$ and $V_{Zn}{}^{1-}$ are shown in figures 3(d)–(g). Note that the spin density is majorly localized on the neighboring O-site, with a minor contribution from the nearest neighboring Zn atoms.

The total DOSs for the ZnO supercell with an O_i^0, O_i^- and O_i^{2-} at the oct site are shown in figures 4(a)–(c) respectively. The spin-up bands are fully occupied while the spin-down bands are partially filled, resulting in the residual magnetic moments per O_i^0 and O_i^-. The O_i^{2-} has symmetric spin up and down densities and thus the supercell containing the O_i^{2-} has zero net magnetic moment. The spin-density distributions for the O_i^0 and O_i^- are respectively shown in figures 4(d)–(g), indicating that the effective spin is majorly localized at the O_i sites. The surrounding Zn and O atoms also contribute to the magnetic moment in the supercell, which is consistent with the projected DOS on O-p and Zn-d orbitals.

The asymmetric DOS' of the $(2V_{Zn} - V_O)^0$ and $(2V_{Zn} - V_O)^-$ in the a-b configuration as shown in figures 5(a) and (b) respectively reveal their non-zero magnetic moment, while the symmetric DOS of the $(2V_{Zn} - V_O)^{2-}$ in the a-b plane configuration as shown in figure 5(c) reveals its non-ferromagnetic nature. Similarly, the asymmetric DOS' of the $(2V_{Zn} - V_O)^0$ and $(2V_{Zn} - V_O)^{1-}$ in the configuration of *c*-axis

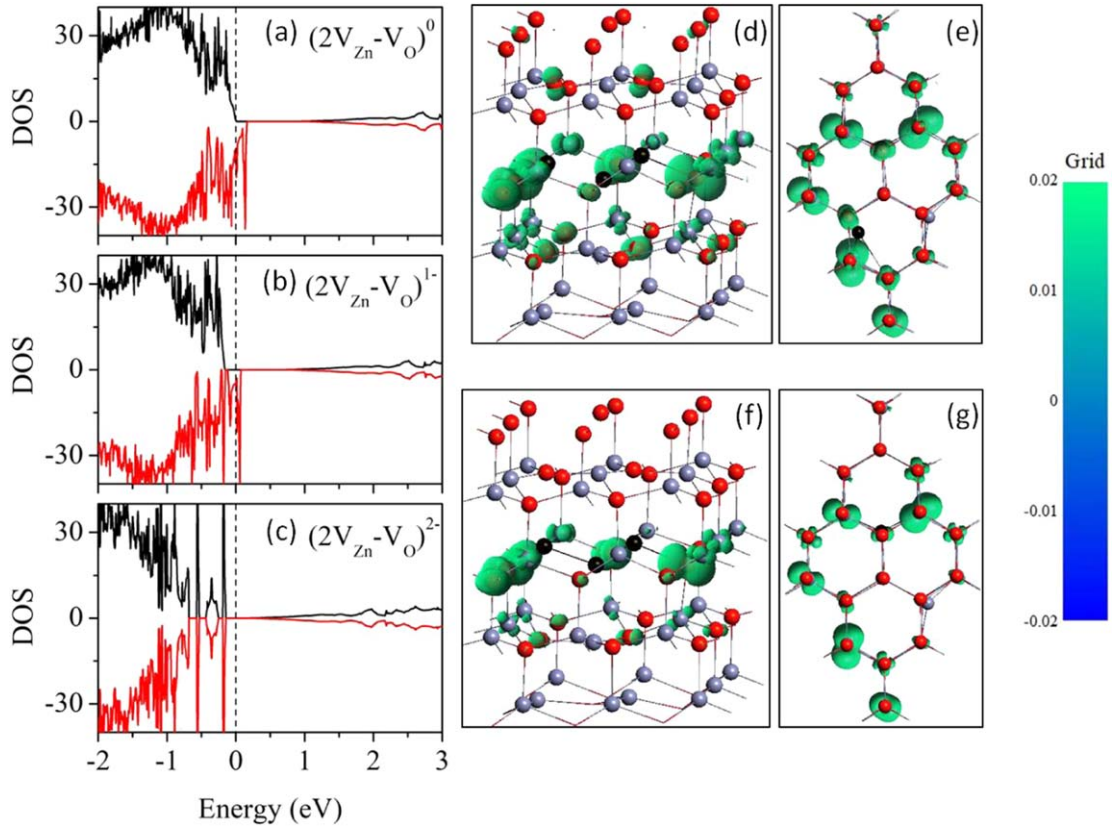

Figure 5. The DOS' of ZnO with the (a) $(2V_{Zn} - V_O)^0$, (b) $(2V_{Zn} - V_O)^{1-}$ and (c) $(2V_{Zn} - V_O)^{2-}$ staying at a-b plane. The spin up (black line) and spin down (red line) DOS is set above and below the abscissa axis. The Fermi-level is indicated by the black dash line at 0 eV. (d) The top view and (e) the side view of the effective spin density distribution for $(2V_{Zn} - V_O)^0$. (f) The top view and (g) the side view of the effective spin density distribution for $(2V_{Zn} - V_O)^{1-}$. The iso-surface value is 0.02 e A^{-3}. The black, red and black balls represent Zn, O and vacancy atoms in supercell respectively.

(figures 6(a) and (b) respectively) reveal their non-zero magnetic moment, while the symmetric DOS of the $(2V_{Zn} - V_O)^{2-}$ in the c-axis configuration (figure 6(c)) shows that its magnetic moment is zero. The top views and side views of the effective spin density distributions for the ferromagnetic $(2V_{Zn} - V_O)^0$ and $(2V_{Zn} - V_O)^{1-}$ in the configurations of a-b plane and c-axis are respectively shown in figures 5(d)–(g) and figures 6(d)–(g) respectively. These effectively spin density distributions have a common feature that the p-electrons around the neighboring and the second neighboring O-atoms, as well as the d-electrons on the neighboring Zn atoms are the major contributors for the spin density. The magnetic moments are localized around the defects.

Discussion

The formation energies of all the native point defects, V_OV_{Zn}, $2V_{Zn} - V_O$ and $2V_O - V_{Zn}$ with different charge states and in the different configurations were calculated. V_{Zn} has the lowest formation energy in the conditions of O-rich, O-poor and regardless of the Fermi level position, and thus V_{Zn} was the most probable intrinsic defect existing in ZnO. Among the vacancy clusters, $2V_{Zn} - V_O$ has the lowest formation energy and in particular for the O-rich condition its formation energy is negative while E_F is close to the CBM.

For the point defects and vacancy clusters that favor FM ordering, the localized moments in the corresponding ZnO supercell strongly depend on the type of defects and the charge states. The magnetic study on the intrinsic point defects and the vacancy clusters showed that V_{Zn}^0 V_{Zn}^-, O_i^0 (oct) and O_i^- (oct), $2V_{Zn} - V_O^0$ and $2V_{Zn}V_O^-$ in both the configurations of *c*-axis and a-b plane had non-zero magnetic moment, and energetically favorable to the FM state as compared to AFM state. Some of the charge states of O_{Zn} and $V_{Zn}V_O$ carried non-zero magnetic moment but their AFM state was energetically more stable than the FM state by 3–4 meV. Among the defects favoring FM states, $V_{Zn}{}^0$ and O_i^- (oct) had the largest energy differences between the AFM and FM states (ΔE), and the highest Curie temperature of 294 K among the others. $V_{Zn}{}^0$ and O_i^- (oct) contribute for 1.82 μB/unit-cell and 1.01 μB/unit-cell respectively. Moreover, their formations energies are

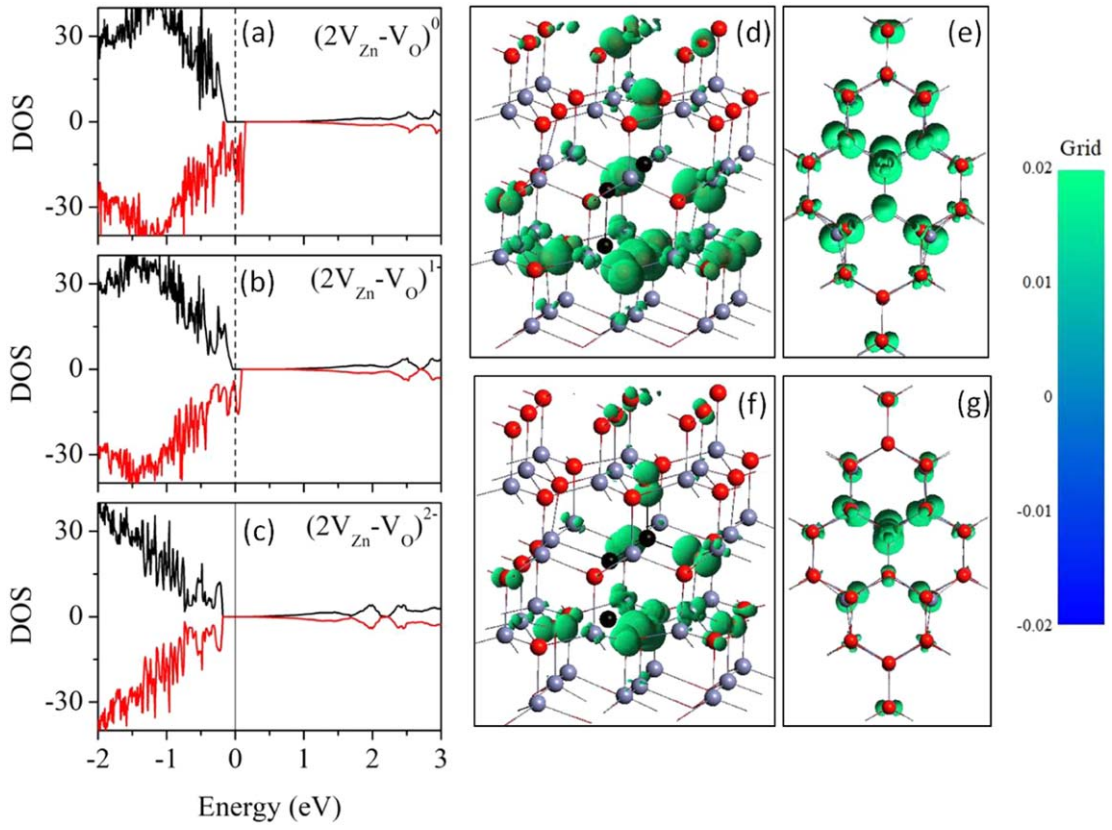

Figure 6. The DOS' of ZnO with the (a) $(2V_{Zn} - V_O)^0$, (b) $(2V_{Zn} - V_O)^{1-}$ and (c) $(2V_{Zn} - V_O)^2$ along *c* axis. The spin up (black line) and spin down (red line) DOS is set above and below the abscissa axis. The Fermi-level is indicated by the black dash line at 0 eV. (d) The top view and (e) the side view of the effective spin density distribution for $(2V_{Zn} - V_O)^0$. (f) The top view and (g) the side view of the effective spin density distribution for $(2V_{Zn} - V_O)^{1-}$. The iso-surface value is 0.02 e A^{-3}. The black, red and black balls represent Zn, O and vacancy atoms in supercell respectively.

low, in particular under the O-rich condition for n-type materials. The $2V_{Zn}V_O$'s in *c*-axis and ab-plane configurations with 0 and −1 charge states also have non-zero localized magnetic moment and favors for FM state, though the ΔE are relatively small and thus resulting in low Curie temperatures. The largest ΔE and highest Curie temperature among the different configurations and charge states for $2V_{Zn}V_O$'s is 29 meV and 224 K respectively, which occurs at the *c*-axis configuration and −1 charge. Thus, $2V_{Zn}V_O$ do not contribute FM effectively at room temperature, while V_{Zn} and O_i could be the probable defects responsible for the observed RT FM in ZnO. Khalid *et al* [33] studied the origin of RTFM in undoped ZnO using a comprehensive approach (SQUID, positron annihilation spectroscopy, x-ray diffraction and first principle calculation) and associated the observed RTFM to V_{Zn}, though there is no experimental report contributing the observed room temperature FM to O_i. However, the ΔE for V_{Zn} is still relatively low and its Curie temperature is marginally close to the room temperature. The thermal stability of its RTFM would not be robust against thermal excitation.

The current study shows that (summarized in table 3) the defects possessing non-zero magnetic moment and energetically favoring ferromagnetic state are all acceptors and the magnetic moments are mainly contributed from the O atoms. It is also noticed that the localized magnetic moments are favored if these defects are filled by a hole in a more positive state. Kenmochi *et al* [34, 35] in first principle magnetic studies of MgO, SrO and BaO suggested that FM originated from double exchange could be correlated with hole doping, for which Yamamoto and Katayama [36] reported that hole-doping was favored by co-doping of donor and acceptor.

To discuss for the undertainties of the current results, it would be worthy to bring to the attention that the T_C estimated by the mean-field approximation does not involve the interaction range, which would lead to significant errors in the dilute magnetic semiconductor with low defect concentration [37]. Therefore, the realistic T_C values could be lower than the ones obtained by the mean-field approximation. Seike *et al* [38] reported that to induce ferromagnetism under homogenous distribution conditions, 15%–20% doping concentration is required for RTFM [38]. In the present study, the corresponding defect concentration is ~2.8% for one defect in the unit cell, which is much lower than the threshold. For the practical fabrication of ZnO samples like film grown by pulsed laser deposition, the native defect like the V_{Zn}-related defect has

concentration of ~10^{18} cm^{-3} (~0.01 %) in undoped ZnO [39]. Besides, the assumption of homogeneity is difficult to be confirmed for realistic DMS systems. Nano-scale inhomogeneity like spinodal decomposition cannot be exclude as the cause of the experimental observation of RTFM in the doped ZnO systems [40, 41].

Conclusion

In conclusion, first principle calculation was performed to systematically study the relaxed atomic geometry, formation energies and magnetic properties of all the native point defects (vacancies, interstitials and antisites) and the vacancy clusters $V_{Zn}V_O$, $V_{Zn} - 2V_O$ and $2V_{Zn} - V_O$ in ZnO. Only the unit cells of ZnO containing the V_{Zn}, O_i (oct) and $2V_{Zn} - V_O$ in the configurations of a-b plane and *c*-axis energetically favors for FM state as compared to AFM state and carry non-zero magnetic moments. The energy differences between the FM and AFM states ΔE, and the magnetic moments depends on the charge state and the defect configuration, varying from 7–38 meV and 0.9–2.0 μB per unit cell respectively. V_{Zn}^{0} and O_i^{-} are the two defects having the low formation energies, the largest ΔE and Curie temperautres (both are 38 meV and 294 K respectively). Their magnetic moments are 1.82 μB per unit cell and 1.01 μB per unit cell respectively. These two defects could be the origins of the experimental observed RTFM in ZnO materials, though their FM states are not robustly stable against thermal excitation to the AFM state as their ΔE's are still relatively small. For the case of $2V_{Zn} - V_O$'s, their ΔE's are even smaller (7–29 meV for different charge states and configurations). The low ΔE leads to the low Curie temperature, which is lower than the room temperature. The formation energies of $2V_{Zn} - 2V_O$'s are larger than those of V_{Zn} and O_i's, indicating their relative lower abundance with the equilibrium situation. $2V_{Zn} - 2V_O$'s are thus not the important contributor to RTFM.

Acknowledgments

This work was financially supported by the HKSAR RGC GRF (project no. 17302115).

ORCID iDs

Cai-Qin Luo https://orcid.org/0000-0003-4368-0627
Si-Cong Zhu https://orcid.org/0000-0003-2103-3998
Francis Chi-Chung Ling https://orcid.org/0000-0003-4757-1065

References

[1] Ohno H, Munekata H, Penney T, Von Molnar S and Chang L 1992 Magnetotransport properties of p-type (In, Mn) As diluted magnetic III–V semiconductors *Phys. Rev. Lett.* **68** 2664
[2] Wolf S, Awschalom D, Buhrman R, Daughton J, von Molnár V S, Roukes M, Chtchelkanova A Y and Treger D 2001 Spintronics: a spin-based electronics vision for the future *Science* **294** 1488–95
[3] Hong N H, Sakai J, Prellier W, Hassini A, Ruyter A and Gervais F 2004 Ferromagnetism in transition-metal-doped TiO_2 thin films *Physical Review* B **70** 195204
[4] Dhar S, Pérez L, Brandt O, Trampert A, Ploog K, Keller J and Beschoten B 2005 Gd-doped GaN: a very dilute ferromagnetic semiconductor with a curie temperature above 300 K *Phys. Rev.* B **72** 245203
[5] Sharma P, Gupta A, Rao K, Owens F J, Sharma R, Ahuja R, Guillen J O, Johansson B and Gehring G 2003 Ferromagnetism above room temperature in bulk and transparent thin films of Mn-doped ZnO *Nat. Mater.* **2** 673–7
[6] Özgür Ü, Alivov Y I, Liu C, Teke A, Reshchikov M A, Doğan S, Avrutin V, Cho S-J and Morkoç H 2005 A comprehensive review of ZnO materials and devices *J. Appl. Phys.* **98** 041301
[7] Dietl T, Ohno H, Matsukura F, Cibert J and Ferrand e D 2000 Zener model description of ferromagnetism in zinc-blende magnetic semiconductors *Science* **287** 1019–22
[8] Yi J, Lim C, Xing G, Fan H, Van L, Huang S, Yang K, Huang X, Qin X and Wang B 2010 Ferromagnetism in dilute magnetic semiconductors through defect engineering: Li-doped ZnO *Phys. Rev. Lett.* **104** 137201
[9] Hsu H, Huang J-C A, Huang Y, Liao Y, Lin M, Lee C, Lee J, Chen S, Lai L and Liu C-P 2006 Evidence of oxygen vacancy enhanced room-temperature ferromagnetism in Co-doped ZnO *Appl. Phys. Lett.* **88** 242507
[10] Herng T, Qi D-C, Berlijn T, Yi J, Yang K, Dai Y, Feng Y, Santoso I, Sánchez-Hanke C and Gao X 2010 Room-temperature ferromagnetism of Cu-doped ZnO films probed by soft x-ray magnetic circular dichroism *Phys. Rev. Lett.* **105** 207201
[11] Yan Z, Ma Y, Wang D, Wang J, Gao Z and Song T 2008a Surfactant-free fabrication of ZnO spheres and pseudospherical structures *J. Phys. Chem.* C **112** 9219–22
[12] Yi J, Pan H, Lin J, Ding J, Feng Y, Thongmee S, Liu T, Gong H and Wang L 2008 Ferromagnetism in ZnO nanowires derived from electro-deposition on AAO template and subsequent oxidation *Adv. Mater.* **20** 1170–4
[13] Liu W, Li W, Hu Z, Tang Z and Tang X 2011 Effect of oxygen defects on ferromagnetic of undoped ZnO *J. Appl. Phys.* **110** 013901
[14] Banerjee S, Mandal M, Gayathri N and Sardar M 2007 Enhancement of ferromagnetism upon thermal annealing in pure ZnO *Appl. Phys. Lett.* **91** 182501
[15] Lin X-L, Yan S-S, Zhao M-W, Hu S-J, Han C, Chen Y-X, Liu G-L, Dai Y-Y and Mei L-M 2011 Possible origin of ferromagnetism in un-doped ZnO: first-principles calculations *Phys. Lett.* A **375** 638–41

[16] Xu Q, Schmidt H, Zhou S, Potzger K, Helm M, Hochmuth H, Lorenz M, Setzer A, Esquinazi P and Meinecke C 2008 Room temperature ferromagnetism in ZnO films due to defects *Appl. Phys. Lett.* **92** 082508
[17] Zuo X, Yoon S-D, Yang A, Duan W-H, Vittoria C and Harris V G 2009 Ferromagnetism in pure wurtzite zinc oxide *J. Appl. Phys.* **105** 07C508
[18] Yan Z, Ma Y, Wang D, Wang J, Gao Z, Wang L, Yu P and Song T 2008b Impact of annealing on morphology and ferromagnetism of ZnO nanorods *Appl. Phys. Lett.* **92** 081911
[19] Xing G, Wang D, Yi J, Yang L, Gao M, He M, Yang J, Ding J, Sum T C and Wu T 2010 Correlated d 0 ferromagnetism and photoluminescence in undoped ZnO nanowires *Appl. Phys. Lett.* **96** 112511
[20] Wang Q, Sun Q, Chen G, Kawazoe Y and Jena P 2008 Vacancy-induced magnetism in ZnO thin films and nanowires *Phys. Rev.* B **77** 205411
[21] Chakrabarty A and Patterson C H 2011 Defect-trapped electrons and ferromagnetic exchange in ZnO *Phys. Rev.* B **84** 054441
[22] Tietze T, Audehm P, Chen Y C, Schütz G, Straumal B B, Protasova S G, Mazilkin A A, Straumal P B, Prokscha T and Luetkens H 2015 Interfacial dominated ferromagnetism in nanograined ZnO: a μSR and DFT study *Sci. Rep.* **5** 8871
[23] Kohan A, Ceder G, Morgan D and Van de Walle C G 2000 First-principles study of native point defects in ZnO *Phys. Rev.* B **61** 15019
[24] Look D C, Reynolds D, Hemsky J W, Jones R and Sizelove J 1999 Production and annealing of electron irradiation damage in ZnO *Appl. Phys. Lett.* **75** 811–3
[25] Tuomisto F, Saarinen K, Look D C and Farlow G C 2005 Introduction and recovery of point defects in electron-irradiated ZnO *Phys. Rev.* B **72** 085206
[26] Dong Y, Tuomisto F, Svensson B G, Kuznetsov A Y and Brillson L J 2010 Vacancy defect and defect cluster energetics in ion-implanted ZnO *Phys. Rev.* B **81** 081201
[27] Kucheyev S O, Williams J, Jagadish C, Zou J, Evans C, Nelson A and Hamza A 2003 Ion-beam-produced structural defects in ZnO *Phys. Rev.* B **67** 094115
[28] Van de Walle C G and Neugebauer J 2004 First-principles calculations for defects and impurities: applications to III-nitrides *J. Appl. Phys.* **95** 3851–79
[29] Janotti A and Van de Walle C G 2007 Native point defects in ZnO *Phys. Rev.* B **76** 165202
[30] Oba F, Togo A, Tanaka I, Paier J and Kresse G 2008 Defect energetics in ZnO: a hybrid Hartree–Fock density functional study *Phys. Rev.* B **77** 245202
[31] Kudrnovský J, Turek I, Drchal V, Máca F, Weinberger P and Bruno P 2004 Exchange interactions in III–V and group-IV diluted magnetic semiconductors *Phys. Rev.* B **69** 115208
[32] Seña N, Dussan A, Mesa F, Castaño E and González-Hernández R 2016 Electronic structure and magnetism of Mn-doped GaSb for spintronic applications: a DFT study *J. Appl. Phys.* **120** 051704
[33] Khalid M *et al* 2009 Defect-induced magnetic order in pure ZnO films *Phys. Rev.* B **80** 035331
[34] Kenmochi K, Ann Dinh V, Sato K, Yanase A and Katayama-Yoshida H 2004a Materials design of transparent and half-metallic ferromagnets of MgO, SrO and BaO without magnetic elements *J. Phys. Soc. Jpn.* **73** 2952–4
[35] Kenmochi K, Seike M, Sato K, Yanase A and Katayama-Yoshida H 2004b New class of diluted ferromagnetic semiconductors based on CaO without transition metal elements *Japan. J. Appl. Phys.* **43** L934
[36] Yamamoto T and Katayama-Yoshida H 1997 Materials design for the fabrication of low-resistivity p-type GaN using a codoping method *Japan. J. Appl. Phys.* **36** L180
[37] Sato K, Schweika W, Dederichs P and Katayama-Yoshida H 2004 Low-temperature ferromagnetism in (Ga, Mn) N: *ab initio* calculations *Phys. Rev.* B **70** 201202
[38] Dietl T, Sato K, Fukushima T, Bonanni A, Jamet M, Barski A, Kuroda S, Tanaka M, Hai P N and Katayama-Yoshida H 2015 Spinodal nanodecomposition in semiconductors doped with transition metals *Rev. Mod. Phys.* **87** 1311
[39] Zilan W *et al* 2019 Vacancy cluster in ZnO films grown by pulsed laser deposition *Sci. Rep.* **9** 3534
[40] Seike M, Dinh V A, Fukushima T, Sato K and Katayama-Yoshida H 2012 Self-organized nanostructures and high blocking temperatures in MgO-based d0 ferromagnets *Japan. J. Appl. Phys.* **51** 050201
[41] Sato K, Bergqvist L, Kudrnovský J, Dederichs P H, Eriksson O, Turek I, Sanyal B, Bouzerar G, Katayama-Yoshida H and Dinh V 2010 First-principles theory of dilute magnetic semiconductors *Rev. Mod. Phys.* **82** 1633